



Geology of Mairan middle dome: Its implication to silicic volcanism on the Moon



Joseph M. Boyce^{a,*}, Thomas Giguere^a, Peter Mougini-Mark^a, Timothy Glotch^b,
G. Jeffrey Taylor^a

^a Hawaii Institute of Geophysics and Planetology, University of Hawaii, Honolulu, HI 96822, USA

^b Department of Geosciences, Stony Brook University, Stony Brook, NY 11794, USA

ARTICLE INFO

Keywords:

Moon
Surface
Silicic
Geological processes
Geologic mapping

ABSTRACT

Mairan middle dome (MMD), a lunar “red spot” of silicic composition, and the surrounding maria were emplaced in the same two major episodes of volcanism. Both episodes at MMD included eruptions of low-FeO, silica-rich lava, while basaltic lava flooded the surrounding terrain during these episodes. MMD is a composite of, at least, seven small volcanic edifices. Crater counts suggest that the first episode occurred at $\sim 3.75 \pm 0.1$ Ga when low FeO, high-silica lavas erupted at MMD, and Mairan T, the small dome 11 km northwest of MMD. At about the same time, basaltic composition lava erupted southeast of MMD. A second major episode of volcanism at MMD occurred at $\sim 3.35 \pm 0.2$ Ga when low FeO, and high-silica lavas erupted at the summits of individual small volcanic edifices and a central plateau area between them. During this phase, mare basaltic lavas again flooded the area surrounding MMD and Mairan T. This sequence of events indicates that the emplacement of MMD is more complex than previously thought. In addition, the simultaneous eruption of basaltic composition lavas and low FeO, high-SiO₂ lavas in this region supports the underplating model for production of magma to form the “red spots” volcanic complexes on the Moon.

1. Introduction

Mairan domes, four Lunar “red spot” surface features, are volcanic constructs located at $\sim 312.3^\circ$ E, 41.4° N in northern Oceanus Procellarum (Fig. 1). These volcanic domes are composed of high SiO₂ and low FeO lava flows (Scott and Eggleton, 1973; Glotch et al., 2011). Until now, their small size and the lack of high-resolution imaging and remote sensing data have hindered further investigation of the geology of these features. However, recent acquisition of high-resolution imaging and other remote sensing data (e.g., Lunar Reconnaissance Orbiter Camera [LROC], and Diviner Lunar Radiometer Experiment (Diviner) thermal data, Kaguya topographic information, and Chandrayaan-1 compositional data) have changed this for Mairan middle dome (MMD), the largest of the Mairan domes. These new data have enabled the detailed characterization and mapping of distinct geologic units on MMD and the surrounding mare based on their morphology, composition, and model crater age. The focus of this study is MMD, the largest of four small domes (Fig. 2).

2. Background and geologic setting

Mairan middle dome is a lunar “red spot” characterized by relatively high albedo, strong absorption in the UV, and is thought to be a volcanic construct produced by non-mare volcanism connected with KREEP basalts or even more evolved highlands composition, such as dacite or rhyolite (Malin, 1974; Wood and Head, 1975; Head and McCord, 1978). These volcanic centers appear to be petrologic anomalies on the Moon that represent strong geochemical departures from primordial compositions, and are indicators of magma processing. Consequently, determining the nature and age of these centers is important for placing constraints on theories of lunar origin, thermal models of the lunar crust, and lunar geologic evolution (Hagerty et al., 2006; Jolliff et al., 2011). Although MMD is relatively small, ~ 11 km across, new high-resolution orbital data facilitate its detailed characterization that enables a much better understanding of its geologic nature and development. This also adds to the overall understanding of the geologic nature of “red spot” volcanic centers (i.e., a volcanic center is a relatively large long-lived volcanic edifice) and provides deeper insight into how they fit into

* Corresponding author.

E-mail addresses: jboyce@higp.hawaii.edu (J.M. Boyce), thomas.giguere@higp.hawaii.edu (T. Giguere), pmm@higp.hawaii.edu (P. Mougini-Mark), timothy.glotch@stonybrook.edu (T. Glotch), gtaylor@higp.hawaii.edu (G.J. Taylor).

<https://doi.org/10.1016/j.pss.2017.12.009>

Received 22 January 2017; Received in revised form 21 August 2017; Accepted 13 December 2017

Available online 15 December 2017

0032-0633/© 2017 Elsevier Ltd. All rights reserved.

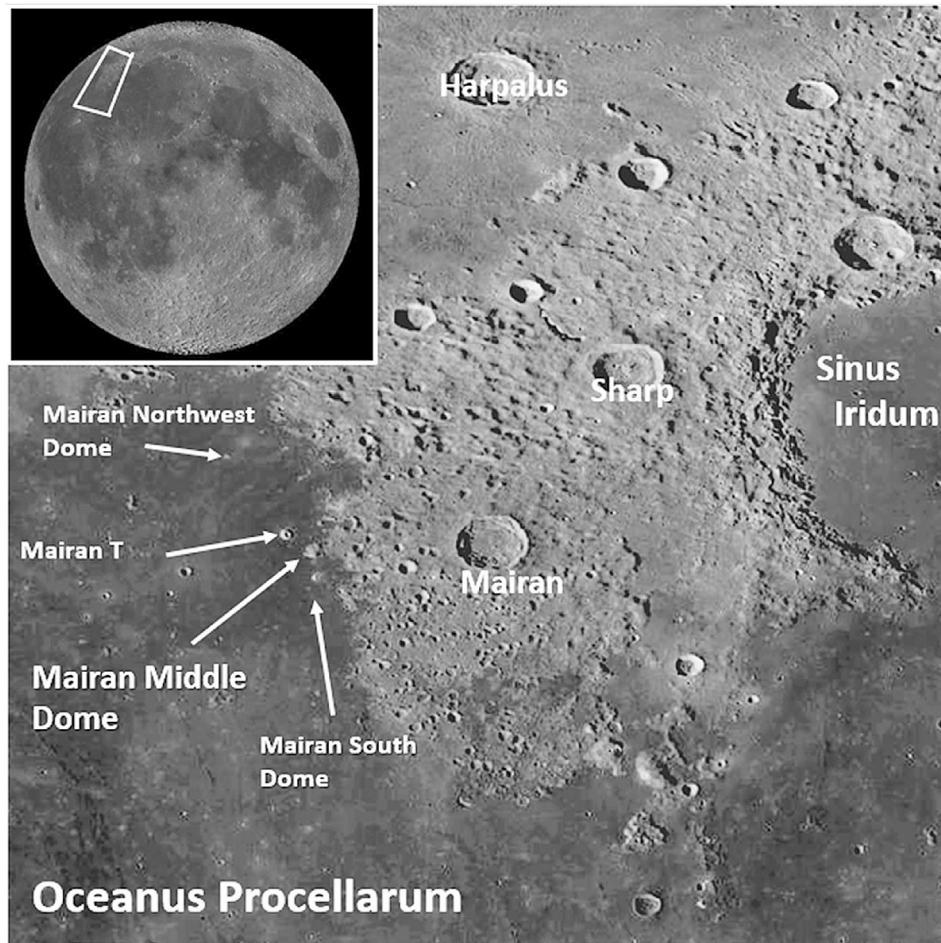


Fig. 1. Portion of northeast Oceanus Procellarum showing the location of the Mairan domes. North is at the top. Image mosaic from the LROC Quick map website.

lunar evolution.

Nearly all red spot volcanic complexes (i.e., a volcanic complex is a persistent volcanic vent area that has built a complex combination of volcanic landforms) on the Moon, except the Compton-Belkovich Volcanic Complex, are located in areas associated with mare. Each of these complexes has its own unique shape that suggests different geologic conditions (e.g., slight difference in composition, gas content, or duration of activity) and history. For example, Mons Hansteen is a two-layer mesa with multiple vents and one satellite cinder cone. The Compton-Belkovich Volcanic Complex, is not associated with mare (Jolliff et al., 2011; Chauhan et al., 2015). It is approximately the same size as Mon Hansteen (Boyce et al., 2017), with a broad area of elevated topography punctuated by a broad central depression. It includes irregular collapse depressions, a variety of dome sizes, and possible lava flows. The Lassell Massif complex includes several geologic units, flow fronts, volcanic cone, and two large volcanic pits (Ashley et al., 2016). It may be partially buried and could be much larger. In contrast, the Gruithuisen domes display two relatively large elongate domes and a small dome, all of which show evidence for being built by a sequence of viscous lava flows (Head et al., 1978; Chevrel et al., 1999). The detailed geologic history, like that presented here for Mairan domes, has yet to be completed for all of these red spot volcanic centers, but would help us to understand why these volcanic centers are so different than other volcanic features on the Moon and what their place is within lunar geologic history.

The Mairan domes include four massifs located at the northern edge of Oceanus Procellarum, west of Mairan crater and east of Rümker hills (Glotch et al., 2011). Three of these domes, Mairan T, Middle and South domes are within ~11 km of each other, while a fourth one (Northwest dome) is about 60 km northwest of the others (Glotch et al., 2011)

(Fig. 2). All of these domes are small, < 12 km across. They are surrounded and embayed by mare, except for the east side of MMD that contacts with the highlands. The exact location of the boundary between MMD and the highlands is not sharp or obvious, possibly a result of degradation by and contamination from impact gardening, preventing determination of their intersection relationships. Based on extrapolation from crater counts for an area west of Mairan T, Hiesinger et al. (2003) estimates the mare surrounding these domes to be $\sim 1.33 \pm 0.19$ Ga. However, based on crater degradation age mapping, Boyce (1976) estimates the maria surrounding MMD is $\sim 3.2 \pm 0.1$ Ga, but with additional older maria units $\sim 3.6 \pm 0.1$ Ga located within a few kilometers to tens of kilometers to its south. Wagner et al. (2002) suggest that the highlands east of the Mairan domes are likely to be composed of Iridium ejecta, and based on crater count data, the estimated model age for these highlands (and hence, the Iridium impact basin) is $\sim 3.84 \pm 0.11$ Ga.

Scott and Eggleton (1973) mapped Mairan T, Middle and South domes as volcanic cumulo-domes and suggested they formed by viscous felsic lava. Scott and Eggleton (1973) also mapped Northwest dome as a volcanic dome, considering it a separate geologic feature from the other Mairan domes. More recently, however, Glotch et al. (2011) proposes that all four domes are related.

Based on Earth-based telescopic multispectral images, Head and McCord (1978) showed that Mairan T, Middle and South domes are spectrally anomalous compared to surrounding mare and highlands material, and that their shape and surface texture is similar to many terrestrial dacitic and rhyolitic domes formed by extrusions of viscous lavas at low rates. Wilson and Head (2003) suggested a yield strength, plastic viscosity, and eruption rates and duration inferred from the morphometric characteristics of these domes that are consistent with the

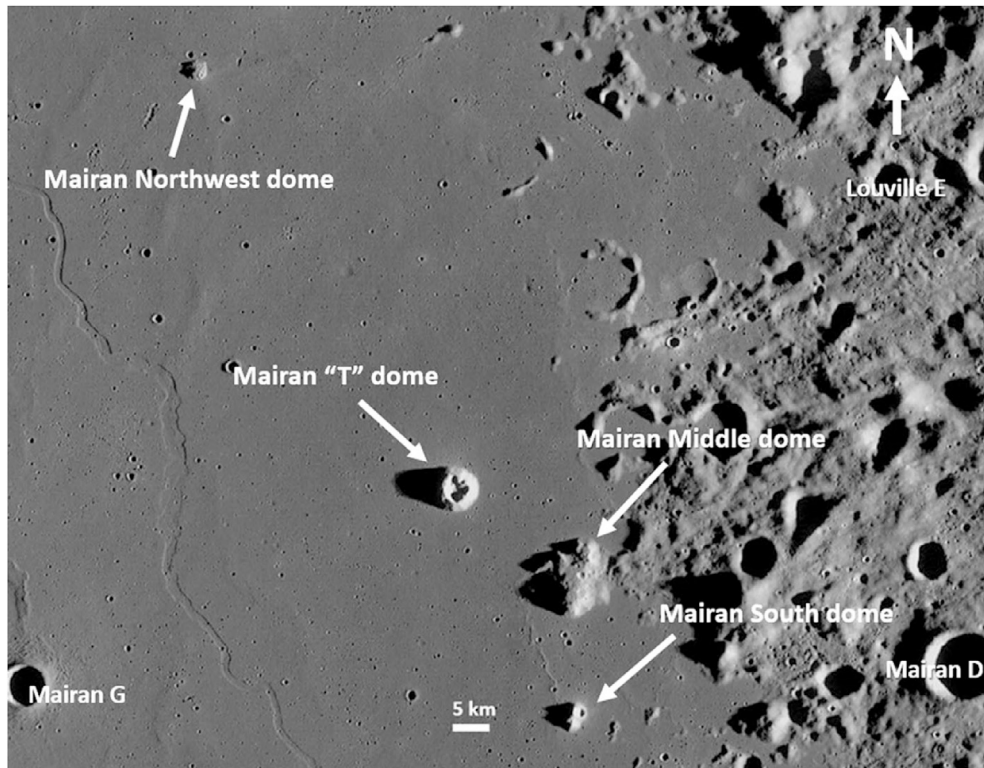


Fig. 2. WAC LROC low sun angle image mosaic from LROC Quickmap website showing the location of Mairan middle dome in relationship to the other Mairan domes in northwest Oceanus Procellarum.

domes forming from magmas with substantially higher viscosity than those typical of mare basalts. Recently Glotch et al. (2011) summarized the remote sensing-derived compositional information about the Mairan domes and noted that MMD exhibits spectral and morphologic attributes consistent with material of felsic composition derivation from a SiO₂-rich, highly evolved magma. They noted that this is in stark contrast to the surrounding basaltic mare and highland units.

3. Results

Our goal is to better understand the geologic nature and history of MMD and its place in the geologic history of the Moon. We use all available, relevant lunar data to conduct detailed image and remote sensing data analysis of MMD and its immediate surroundings. Results of these analyses were used to define and map major geomorphic and compositional units, as well as determine their chronology and absolute

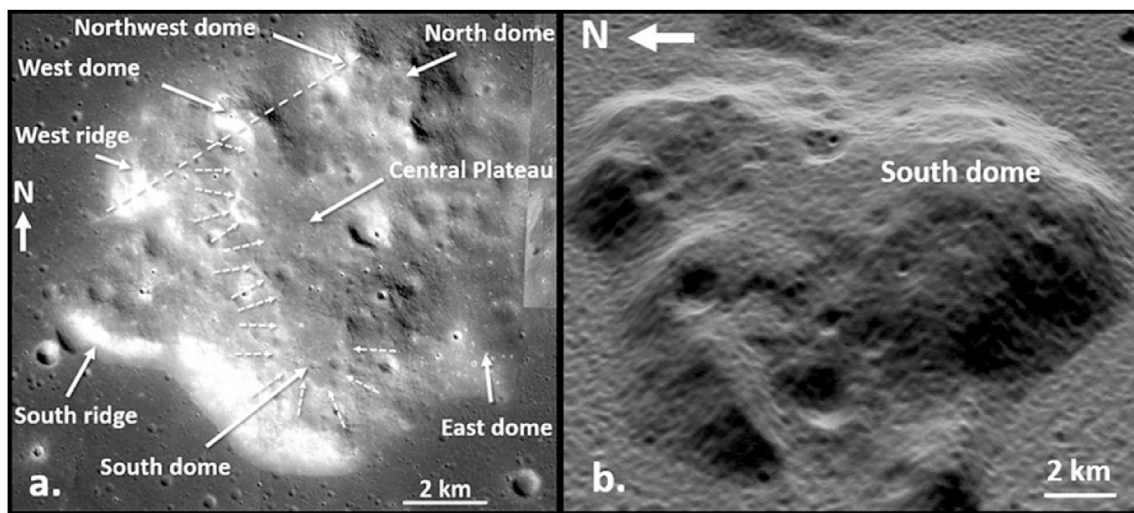


Fig. 3. (a) Is a mosaic of LROC NAC images of Marian middle dome (frame numbers M1099158407L, M1099158407L and M1099165551L). White arrows point to each of MMD's major domes, ridges and its central plateau in this image. Small, white, dashed arrows mark the location of a ~10 m high lobate scarp along the west side of the central plateau on MMD that runs from South dome to West dome. This lobate scarp may be the edge of a lava flow composed of high Si, viscous lavas. A dashed line also runs along the axis of West ridge and intersects the summits of West dome and Northwest dome. This line is possibly the location of a fracture that acted as conduit for magma that erupted to build MMD's West ridge, West dome and Northwest dome. (b) Is an oblique view (from the west, with north to the left) of MMD constructed from shaded-relief Kaguya stereo image data. This image clearly shows that MMD is composed of a central plateau area surrounded by seven relatively small mounds (the largest, South dome, is labeled to aid in interpretation). These mounds are probably small volcanoes. Image derived from Kaguya DTM_Maps02_N23E312N39E315SC.

model crater age.

3.1. Morphology

LROC Wide Angle Camera (WAC) and Narrow Angle Camera (NAC) (Robinson et al., 2010) images and high-resolution topographic data (LROC GLD100 and SELENE Kaguya stereo image data) were used as a basis for characterizing the morphology and morphometry of MMD for this study. These data show that MMD, the largest of the Mairan domes, is a ~ 11.7 km \times ~ 10.7 km dome shaped massif with a maximum relief of ~ 811 m. However, MMD is not a smooth dome, but includes, at least, seven small, relatively closely spaced, domical hills and ridges (Fig. 3). The slopes of these small domes and ridges intersect to produce the current irregular, lumpy shape of MMD. We suggest that these individual small hills and ridges are small volcanic constructs developed over different closely spaced vents, although it also should be recognized that they may be parts of larger volcanic constructs that form MMD.

Of these hills and ridges on MMD, the largest is located on the southern edge (Figs. 3 and 4) and is labeled South dome (names of small domes in this section refer to the hills on MMD and not to the Mairan domes in general). South dome is a steep-sided (slope of $> 22^\circ$ on its south side) relatively symmetrical dome, ~ 6.5 km across, and ~ 811 m high (above the surrounding mare). Located along the east side of South dome is East dome, a low, dome-shaped massif ~ 3.5 km across, and ~ 200 m high. On the southwest side of South dome is South ridge. This southwest-northeast trending ridge is ~ 3 km long, ~ 1 km wide and ~ 150 m high. North dome, located on the north side of MMD is a relatively small (i.e., ~ 3.5 km across and ~ 450 m high) compared with South dome. The eastern flanks of North dome, north of East dome, contain numerous pits that can be as large as ~ 1 km across. Most of these pits are irregularly shaped, although some are circular. To the west of North dome is a much smaller dome (i.e., ~ 2.5 km across and ~ 400 m high), Northwest dome. Both of these small domes have steep slopes ($\sim 22^\circ$ on their northern sides). Separating these domes from West dome on their southwest sides is a short (~ 3 km long) northwest-southeast trending valley. West dome, located on the south side of this valley, is a ~ 3.5 km across, ~ 400 m high dome. A lobate scarp (~ 10 m relief) runs around most of the west and north sides at ~ 350 m elevation level (see Fig. 3). This scarp may be the edge of a silica-rich lava flow. To the south of West dome and separated from it by a ~ 1.0 km diameter pit (of likely volcanic or collapse origin) is West ridge. This northeast-southwest trending ridge is ~ 4.5 km long, ~ 350 m high (at its highest). This ridge

may be an extension of West dome and not a separate volcano. The crest of West ridge is on a line with the summits of North dome and West dome (Fig. 3). This may suggest a fracture along this line which served as a conduit to these possible vents.

In central MMD, a ~ 10 km², relatively flat plateau area sits at ~ 400 m above local datum (Figs. 3 and 4). This area is located between South, North, and West domes (Fig. 3), and could be a saddle region between the individual domes formed by a succession of interleaved larger flows from the surrounding small volcanoes, a major flow from South dome, or sagging between domes from internal cooling and collapse. This area is also the location of the largest crater (i.e., ~ 1.2 km diameter) on MMD. While numerous smaller impact craters cover MMD, the origin of this crater is uncertain, but its irregular shape suggest that it may be of volcanic origin, possibly of explosive origin as evidenced by its raised rim. A low relief, hummocky area is located on the southwest side of MMD. West and South ridges, and South and West domes bound this area on the MMD sides (Fig. 3). This area contains numerous pits, some of which are circular, while most are irregular shaped (Fig. 5). These pits may be of volcanic origin, although whether of collapse or explosive origin cannot be determined with the available data.

Like other lunar “red spot” features interpreted to be volcanic domes, the surface of MMD lacks obvious lava flow fronts like those produced by basaltic composition lavas. But, there are features similar to those identified on other “red spot” volcanic centers as high-silica, high-viscosity flows (e.g., see Head et al., 1978; Hawke et al., 2003; Jolliff et al., 2011; Glotch et al., 2011; Ashley et al., 2016). We suggest an example is the lobate scarp that bounds the Central Plateau near the eastern side of South dome (see Fig. 3). This scarp may be the front of a viscous lava flow (Fig. 6). In addition, West dome may not be a separate volcano, but just the northern extension of West ridge.

The presence of bench craters (Fig. 7) as small as ~ 12 m– ~ 15 m diameter suggests that a ~ 3 m to ~ 4 m thick regolith has likely developed on MMD (Oberbeck and Quaide, 1967). Considering the depth/diameter relationships of these small bench craters (Melosh, 1989), their size suggest a strength discontinuity occurs at a depth of $> \sim 3$ m– ~ 4 m of the type produced by a regolith. This suggested thickness is approximately the thickness expected for a regolith produced by impact gardening under the flux of impacts on the surface of the modeled age of MMD (see sections 3.3) (Moore et al., 1980). In addition, the size of bench craters on the surrounding mare just west and north of MMD is similar to those on MMD, suggesting the regolith on that mare is approximately the same thickness as the regolith on MMD.

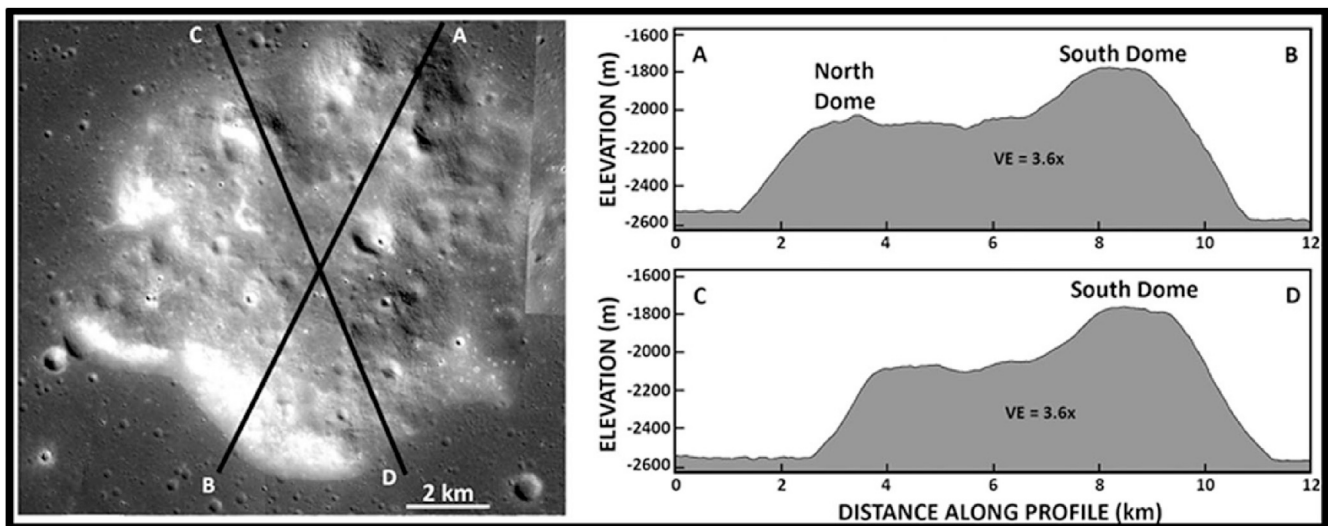


Fig. 4. Topographic profiles across MMD. Left: LROC WAC mosaic (same image as Fig. 3) of MMD that shows the location of topographic profiles, A-B, and C-D. Right: Profiles A-B and C-D were constructed from Kaguya stereo image data and clearly show the central plateau and the prominent massifs, South dome, as well as North dome. The vertical exaggeration (VE) is noted on each profile.

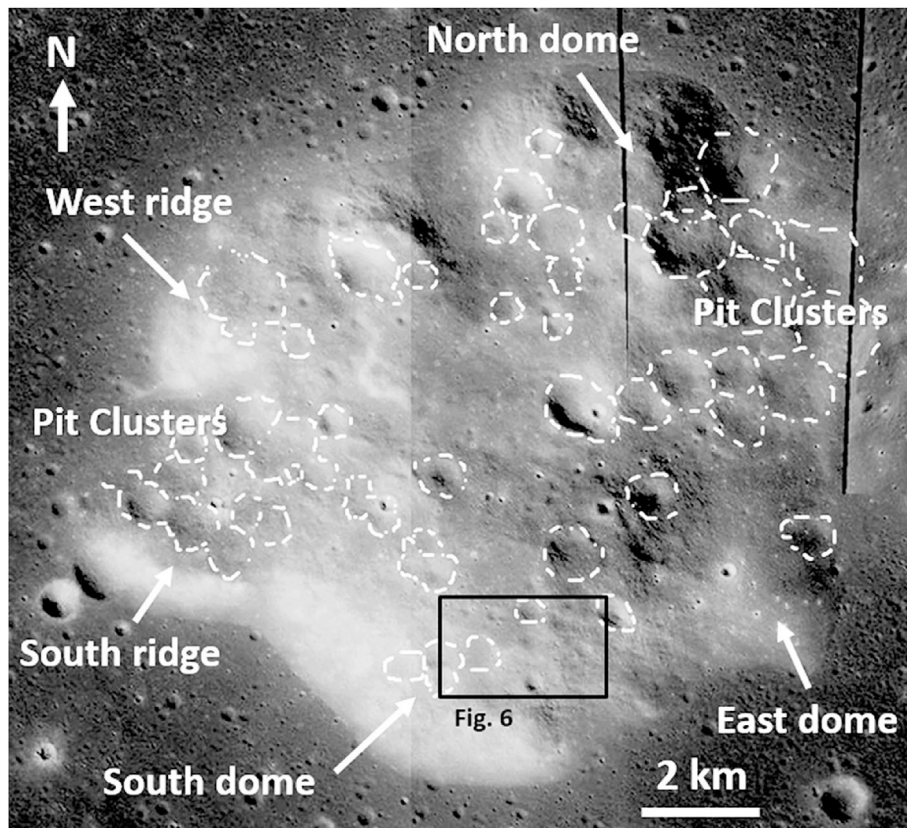


Fig. 5. LROC WAC image mosaic of MMD (same as in Fig. 3) showing the location of pits > ~250 m across. These pits are circled in white dashed lines. We suggest that these pits are likely of volcanic origin because of their irregular shapes, lack of raised rims, and tendency to cluster (i.e., possible chains). Note that closely spaced pits form clusters that occur in low areas on the northeast and southwest sides of MMD. A black box outlines the area shown in Fig. 6.

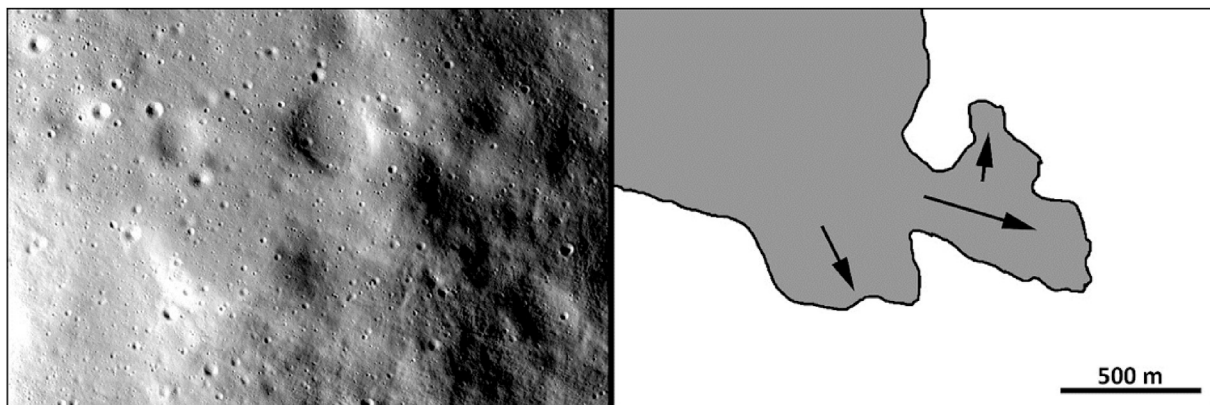


Fig. 6. Potential degraded lobate lava flow front on the eastern flank of South dome of MMD. Left: Part of LROC M1188656127L. Right: Inferred flow direction and extent. Both illustrations are at the same scale, and north is at the top of both. See Fig. 5 for location.

LRO Diviner rock abundance measurements (Fig. 8) and visual examination indicate that there are relatively few boulders and blocks on the surface of MMD, even around relatively fresh impact craters. This is in contrast to the surrounding lunar maria where blocks and boulders are common, especially around fresh impact craters. This lack of boulders on MMD could be the result of mantling by a thin blanket of pyroclastic material on MMD that likely would not contain blocks and would also shield the bedrock from impact quarrying to produce blocks. However, this ash layer would have to be coincidentally approximately the thickness of a regolith predicted by the impact flux corresponding to the age (see Section 3.3) of the surface. Alternatively, the surface of MMD could be composed of materials that are readily broken into small particles by impact gardening to produce a rock free ash like layer. For example,

small impacts formed in flow-generated, rubbly, porous breccia that commonly surface silica-rich lava flows on siliceous domes (see Duffield et al., 1999) would expend a substantial amount of their energy crushing the rubble into fine particles instead of penetrating the layer and excavating rock beneath (Housen and Holsapple, 2012).

Pits are common on MMD. They range in size from the limit of image resolution up to 1.2 km diameter and in morphology from circular, individual pits with raised rims and surrounding deposits that thicken toward the pits rim (see Fig. 7) to subdued, irregular-shaped, rimless pits with no discernible rim deposits extending outward from their rims (Fig. 5). The irregularly shaped pits generally are >250 m diameter, and commonly found in clusters in low area such as the low-relief area bound by West and South ridges, and South and West domes, and along the

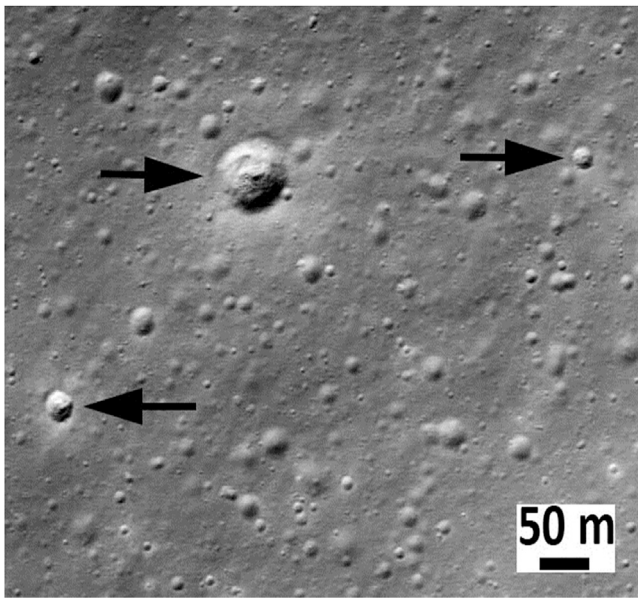


Fig. 7. Examples of small bench craters and flat floor craters located on the central plateau of MMD. Craters marked with arrows exhibit either a flat floor or bench suggesting that they encountered a more resistant layer at depth during their excavation. The size of such small craters, generally regarded as indicating the depth of the regolith, suggests the depth of the resistant layer (i.e., regolith) here may be ~3–4 m. This is approximately the same thickness as the regolith on the surrounding mare of about the same age. The image is from LROC image M173225862L.

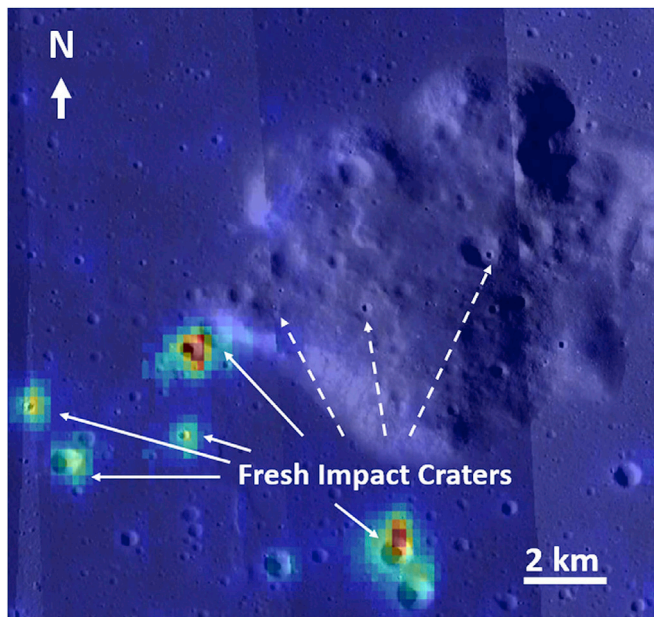


Fig. 8. Diviner surface rock abundance (i.e., blocks or boulders ≥ 1 m) map of MMD superposed on the same LROC NAC mosaic as in Fig. 3. This map shows areas of high rock abundance (reds, greens and yellows) compared with low rock abundance (dark blue). High rock abundances are associated mainly with fresh impact craters on the surrounding mare (white arrows). However, this relationship does not appear to hold for MMD (see dashed white arrows), where small, relatively fresh impact craters on MMD (each has raised rims, distinct ejecta deposits, and one even has rays) exhibit approximately the same low rock abundance as the rest of MMD. Diviner data from LROC Quickmap. (For interpretation of the references to color in this figure legend, the reader is referred to the Web version of this article.)

eastern flank of North dome and East dome. Because of their subdued, irregular shape and association with a volcanic complex, we suggest these pits are probably of volcanic origin, although their morphology has

many (except for obvious ejecta deposits) similarities with impact craters in secondary crater clusters (Oberbeck and Morrison, 1974; van der Bogert et al., 2015). If these pits are volcanic, then they are not as closely spaced as the pits of the pit clusters, (i.e., their rims commonly touch) in central Mons Hansteen (Boyce et al., 2017), the young massif unit at Lassell Massif (Ashley et al., 2016), or the flanks of Gruithuisen domes. This may suggest that the process that produced the pit clusters on these other silica-rich volcanic center did not operate on MMD, or at least, to the same degree. In addition, while we suggest that the irregular pits are volcanic features, we also suggest that the circular, pits with raised rims and surrounding deposits (some with rays) are likely impact craters. The morphology of these pits, for the most part, meet the criteria for being impact craters produced hypervelocity impact (Melosh, 1989).

3.2. Composition

A combination of remote sensing data of the Mairan domes from the LRO Diviner, Kaguya (SELENE) Spectral Profiler (SP), Chandrayaan-1 Moon Mineralogy Mapper (M^3), Lunar Prospector (LP) gamma-ray spectrometer (GRS), and high resolution LRO LROC, WAC and NAC images suggest that the Mairan domes are, indeed, silicic volcanic constructs (see Glotch et al., 2011). Images and spectra of the domes show that they exhibit much higher overall reflectance and silica content than the surrounding terrain suggesting the presence of bright, silicic minerals, and a lack of mafic minerals.

In their synthesis of imaging and remote sensing data and previous finding of the Mairan domes, Glotch et al. (2011) conducted forward modeling of Lunar Prospector GRS data to increase the spatial resolution. This was done by allowing compositional estimation of individual geologic units (Lawrence et al., 2005; Hagerty et al., 2006). The forward modeling technique combined data from remote sensing missions, morphologic data, and sample-based data to obtain information about elemental abundance of features smaller than the spatial resolution of the Lunar Prospector GRS data. They found that MMD has an optimum Th value of 48.0 ± 6 ppm, with the other domes (i.e., Northwest, Mairan T, and South) having optimum Th values of 8.8 ± 3 ppm, 36.5 ± 9 ppm, and 82.8 ± 19 ppm, respectively. These Th values are consistent with terrestrial rhyolites that occur as bi-modal pairings with basalts.

Based on Clementine multispectral imagery (Lucey et al., 2000a), Glotch et al. (2011) found that the FeO abundances of the Mairan domes ranges from 6–10 wt. % FeO, and the surrounding mare basalts range from 15 wt. % to 18 wt. % FeO. When compared to values in the lunar sample suite, Glotch et al. (2011) note that these Th and FeO values for MMD are consistent with alkali-suite lithologies such as granites, felsites, and quartz monzodiorites (Jolliff, 1998; Korotev, 1998; Papike et al., 1998).

Glotch et al. (2011) also reported that M^3 and SP data are consistent with a silicic composition for the domes. They note that the near infrared reflectance (NIR) data exhibits only weak ferrous iron absorptions in the 1 and 2 mm regions, as would be expected for silicic features because the NIR is insensitive to Fe-free minerals. As a result, the lack of strong bands in the SP are consistent with the presence of abundant Fe-free minerals.

Global silicate mineralogy mapping of the Moon from the Diviner aboard LRO (see Greenhagen et al., 2010; Paige et al., 2010) showed that most lunar terrains have spectral signatures consistent with known lunar basalts and anorthosites, but small areas of highly evolved, silica-rich materials are also present on the Moon. Using these Diviner data, Glotch et al. (2010) showed that the mid-infrared spectra of four of the “red spots” (Mons Hansteen, Lassell, Gruithuisen domes, and Aristarchus) could best be explained by quartz, silica-rich glass or alkali feldspar content, consistent with lunar granites in Apollo samples. It should be noted that, effects such as variations in illumination, viewing geometry and soil maturity can add uncertainty to use of these new maps (see Paige et al., 2010). In addition, because the Diviner data make use of only 3 spectral bands (i.e., the three “8 μ m” channels of Diviner) it is difficult to place absolute SiO_2 abundances on Diviner measurements,

even though the spectra from Diviner are still diagnostic of quartz, and other high-SiO₂ minerals such as K-feldspar and plagioclase more sodic than labradorite.

Later, Glotch et al. (2011) focused on the Mairan domes determining their representative spectra to produce a Diviner concavity map using Diviner data to place broad constraints on the composition of the domes. They used Diviner data acquired between 10 am and 2 pm local time between July 2009 and April 2011 with emission angles of <8° binned in 128 pixels per degree based on the three “8 μm” channels of Diviner. To gain insight into the composition of the domes, in particular the SiO₂ content, they employed a simple linear mixing model using quartz as an end-member and augite, anorthite, or microcline as the second end-member (see Glotch et al., 2010, 2011 for details of the model). For this modeling, quartz can be taken as a proxy for any SiO₂ phase. The results of this modeling suggest material on MMD have (1) a quartz content of 70% with an augite content of 30%, (2) a quartz content of 91% and an anorthite content of 9%, or (3) a quartz content of 73% with a microcline content of 27%. Employing this same modeling approach to the surrounding mare suggests that quartz (i.e., SiO₂) ranges from 0% to 30%, considerably less than MMD and consistent with basalt.

In this study, to better define compositional units and their boundaries on MMD, we have generated new higher spatial resolution compositional maps of MMD using LRO Diviner Christiansen feature (CF) map data (see Greenhagen et al., 2010; Glotch et al., 2010, 2011) and Clementine spectral data (see Lucey et al., 2000b; Hawke et al., 2003) that can be processed further to provide better spatial resolution maps (Fig. 9). These maps provide a means of gaining deeper insight into the spatial variations in silica and FeO content on the Moon.

We have sampled the CF map data (see Greenhagen et al., 2010) for MMD and the surrounding mare at 256 pixels per degree (ppd), a substantial improvement over the past processing at 128 ppd, which only slightly oversamples the native resolution of the Diviner ground footprint. In producing this map, and to compensate for the effects of high SiO₂ on high concavity values, CF values > 9 μm (indicative of a positive concavity index) in the area of MMD have been calculated at a more

realistic 7 μm which is more appropriate for silicic compositions. The resultant map is shown in Fig. 9a and suggests that lower elevation areas generally have relatively lower SiO₂ content (green to greenish yellow), and areas at the summits of the small domes, and ridges as well as the east flanks of the central plateau generally exhibit relatively highest SiO₂ content (light to dark blue). The surrounding mare (yellow to red) shows a comparatively lower SiO₂ content.

The technique used to produce the high-resolution FeO map in this study was identical to that described by Hawke et al. (2003) using Clementine five-color digital image model data (Isbell et al., 1999; Eliason et al., 1999; Robinson et al., 1999). These data were mosaicked to produce an image cube in orthographic projection at 100 m/pixel spatial resolution, instead of previous maps at 256 m/pixel. We applied the algorithms of Lucey et al. (2000a, 2000b) to these data to produce a high-resolution FeO content map for MMD (Fig. 9b). This map shows that the surface materials on MMD range in FeO values from ~7 ± 1 wt. % (orange) to ~13 ± 1 wt. % (dark green), and that the wt. percentage of FeO varies systematically across the surface. Materials with the lowest FeO wt. percent values occur at the highest elevations (and along the flanks of the central plateau), while materials highest in FeO content generally occur at the lowest elevations. In addition, consistent with the findings of Glotch et al. (2011), these new data show the maria surrounding MMD has a FeO content of ~17 ± 1 wt. % FeO.

3.3. Crater count ages

The compositional variations discussed in Section 3.2, and landforms in Section 3.1 suggest that MMD is constructed from multiple distinct units that may have formed over an extended time. We have turned to impact crater density-based techniques in order to gain deeper insight into how these units relate to the geologic development of one another, the surrounding region, and the Moon. Crater count data are a relatively reliable means of determining relative age, and with certain assumptions, a reasonable means of estimating absolute (model) age (see Michael and Neukum, 2010). Impact crater density data collected for this purpose in

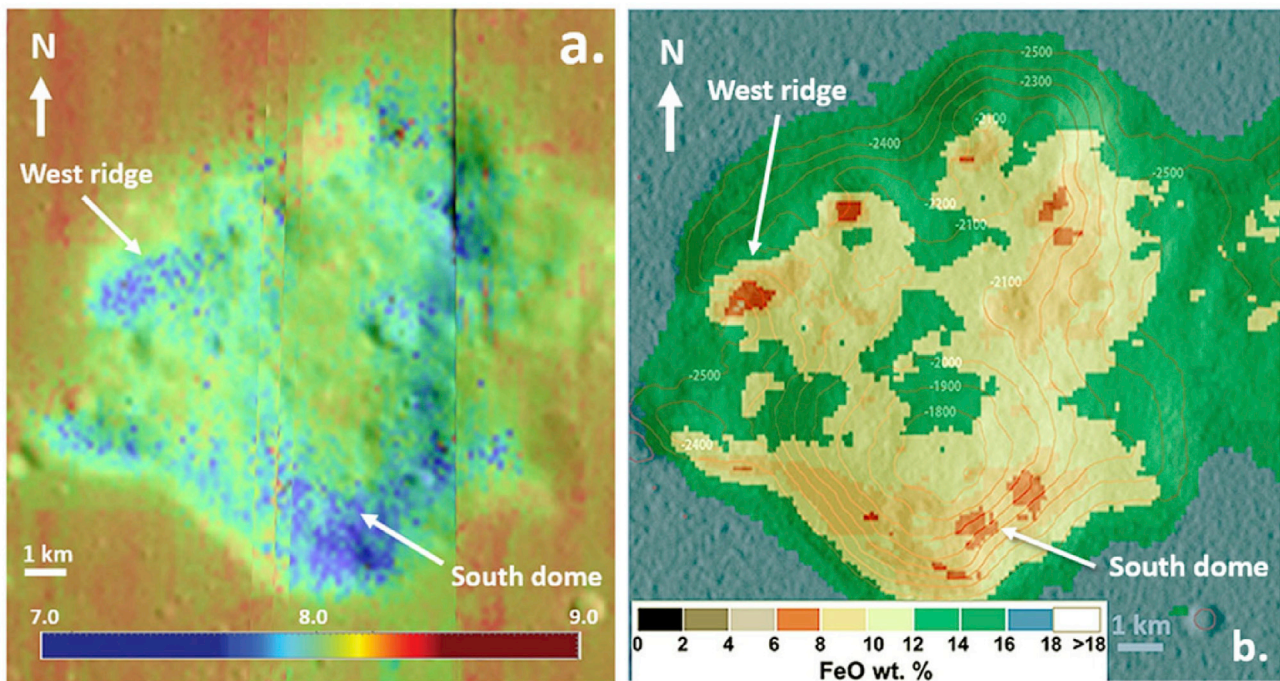


Fig. 9. Compositional maps of MMD. (a.) Diviner Christiansen feature (CF) map at 256 pixels/degree. While an absolute value scale for SiO₂ content cannot be constructed directly for this map the modeling results by Glotch et al. (2011) of Diviner three band spectra show a range in composition on MMD of 70%–91% (blues and greens) SiO₂ and the surrounding mare of ~0–30% (yellow to red) SiO₂ content. The Diviner CF map is superposed on an LROC WAC mosaic. (b.) 100 m/pixel map of the FeO distribution from Clementine data (superposed on the Kaguya based topographic shaded relief map with 100 m contours). Note that the highest SiO₂ and lowest FeO values are generally in the areas of the summits of MMD.

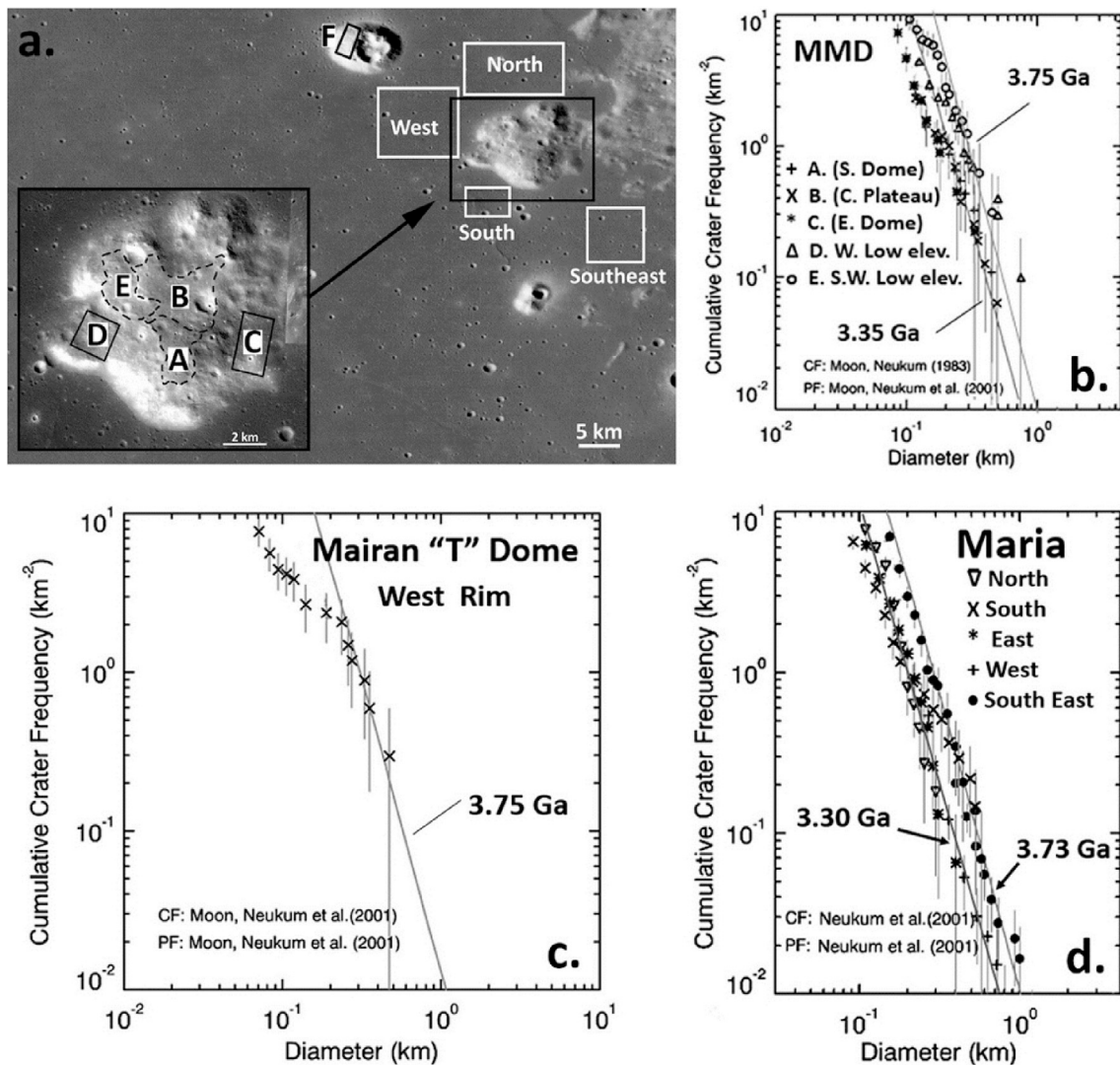


Fig. 10. Crater count data for MMD and surroundings. (a.) Areas where impact craters were counted located on the LROC WAC mosaic. The cumulative size frequency distributions of craters counted in areas shown on the mosaic are plotted in diagrams b, c, and d. (b.) the CSFD for areas A (N = 26, area = 14 km²), B (N = 37, area = 28 km²); C (N = 58, area = 15 km²); D (N = 45, area = 10 km²); and E (N = 52, area = 14 km²) on MMD. (c.) the CSFD (N = 42, area = 5 km²) for Mairan T rim (area F). (d.) the CSFD for mare areas north (N = 143, area = 151 km²), south (N = 101, area = 14 km²), west (N = 71, area = 151 km²), and southeast (N = 88, area = 181 km²) of MMD. N is the number of craters (N) counted in each area, and area is the surface area counted in square kilometers. Error bars were calculated for N in each diameter bin based on only the statistical error inherent to the number of craters counted, assuming a Poisson distribution of values. Diagrams of the CSFD of the crater counts were produced using the program of Michael and Neukum (2010).

the sample areas are shown in Fig. 10a. These sample areas include five on MMD, one on the summit of Mairan T, and four areas on the surrounding maria. LROC NAC high-resolution images were used as the primary data base from which to measure crater diameter for the crater counts. Cumulative size-frequency distribution (CSFD) curves were constructed from the crater count data collected for each sample area and crater model ages were calculated based on the CSFD curve using the craterstats2 program of Michael and Neukum (2010). Error bars, based on the statistical error inherent to the number of craters counted (assuming a Poisson distribution of values), were calculated for the number of craters in each diameter bin (N). The lunar production function and lunar chronology of Neukum et al. (2001) was used to estimate model crater age for the CSFD curves. Care was taken to insure that each sample area contained enough area to insure that the impact crater production function could be confidently determined, and that these areas were flat and horizontal enough to insure that the effects of slope and mass wasting on the crater population were not significant (van der Bogert et al., 2015). While generally all impact craters > ~90 m diameter were included in the counts, rimless and irregular-shaped craters and craters occurring in chains were excluded because they are likely either

endogenic (i.e., volcanic), or are secondary impact craters. However, their effects on the CSFD are generally predictable which also could provide valuable information about the history of the surface (Schultz et al., 1977; Hartmann et al., 1981; van der Bogert et al., 2015). It should also be noted that considering the crater model age (i.e., crater density) of each area counted, the youngest area counted should have a steady-state crater saturation size of ~100 m and the oldest area ~165 m diameter (Moore et al., 1980). This would affect the CSFD of the crater populations below these values, and probably a few tens of meters diameter above these values too, resulting in a roll-over or shallowing of the CSFD curve below these diameters (see Hartmann et al., 1981).

The CSFDs for the craters counted in the five sample areas on MMD (A – E) are plotted in Fig. 10b. The CSFD of craters in three of these areas, i.e., the summit of South dome (area A.), and East dome (area B.) as well as the central saddle (area C.) fall along the same lunar production function with a model age of ~3.35 ± 0.2 Ga (see Michael and Neukum, 2010). In these sample areas, the CSFD curves of craters < ~175 m diameter have shallower negative slopes than the lunar impact production function of larger craters in these areas. This is possibly because the crater population < ~100 m diameter is below the crater saturation size

for this age surface, and up to ~175 m diameter partially effected by it (Moore et al., 1980). It also could be a result of properties of the surface materials that effects small craters more than large craters in these areas. For example, the presence of a weak surface layer produced by a thick regolith or pyroclastic material could cause such a curve roll-over. However, the small size of the bench craters shown in Fig. 9 is inconsistent with this possibility and should only effect the population of crater smaller than a few tens of meter diameter (Hartmann et al., 1981; van der Bogert et al., 2010).

The CSFD of impact craters in the other two areas on MMD, i.e., D and E (both located west of South dome, and the central plateau) approximately fall along the same lunar production function with a model age of $\sim 3.75 \pm 0.1$ Ga. In these two areas, the CSFD curves of craters $< \sim 200$ m diameter also exhibit a shallower negative slope than the lunar impact production function. This probably results for the same reason as the shallow negative slope of the CSFD for small craters in areas A, B and C.

In addition to MMD, and for context reasons, we counted craters on the relatively flat surface near the summit of Mairan T (area F). The resultant CSFD is plotted in Fig. 10c and shows that the population of crater $> \sim 200$ m diameter fall along the lunar impact crater production function for a model age of $\sim 3.75 \pm 0.1$ Ga, similar to sample areas D and E on MMD. However, like the CSFD of small craters on MMD, the CSFD of relatively small impact crater ($< \sim 200$ m diameter) on Mairan T exhibit a shallower negative slope than the lunar impact production function of craters and of the oldest units on MMD. But, the degree of this shallowing exhibited by the CSFD curve for crater < 200 m diameter is much greater than that of the CSFD of areas D and E. This characteristic is most consistent with the effects of a weak surface layer on Mairan T such as would be produced by a pyroclastic mantle or thick regolith (Hartmann et al., 1981; van der Bogert et al., 2010). (It should also be noted that this exercise could not be done for Mairan South dome because a flat and horizontal area of sufficient size for a statically meaningful crater count does not exist there.)

Craters were also counted in four sample areas on the mare near MMD (labeled North, West, South and Southeast in Fig. 10a). The CSFD for these are plotted in Fig. 10d, and show that the mare southeast of MMD has a model crater age of $\sim 3.73 \pm 0.1$ Ga, while the maria north and west of MMD both have a model crater age of $\sim 3.30 \pm 0.2$ Ga. It should be noted that these ages are in contrast to the 1.33 Ga model age extrapolated from crater counts over 50 km east of MMD (Hiesinger et al., 2003), but consistent with the crater degradation age of $\sim 3.2 \pm 0.1$ Ga reported by Boyce (1976) for the maria surrounding MMD, and for a mare unit of $\sim 3.6 \pm 0.1$ Ga southeast of the three main Mairan domes. The south sample area appears to be at a transition between these two different mare age units and shows the effects of this in its CSFD. The CSFD curve of craters in the south sample area is offset at ~ 300 m diameter producing two parallel segments with craters $> \sim 300$ m diameter falling along a lunar production function with an estimated model age of $\sim 3.73 \pm 0.1$ Ga. The segment of this curve with craters ranging from ~ 300 to ~ 125 m diameter falls along a production curve for a model age of $\sim 3.30 \pm 0.2$ Ga. This type of CSFDs curve is commonly a result of partial resurfacing (Hartmann et al., 1981). It suggests that two distinct mare flooding or pyroclastic eruptive events occurred on the mare south of MMD, one at 3.73 ± 0.1 Ga, and a later one at $\sim 3.30 \pm 0.2$ Ga which erased craters $< \sim 300$ m diameter.

4. Geologic history

As with previous investigations (Scott and Eggleton, 1973; Head and McCord, 1978; Wilson and Head, 2003; Robinson et al., 2010; Wagner et al., 2010; Glotch et al., 2011), we suggest that MMD is a ~ 11.7 km \times ~ 10.7 km volcanic dome composed of low-FeO, silica-rich viscous lava flows. Our detailed analysis of the morphologic and compositional characteristics of MMD suggests that this irregular-shaped dome is a composite of at least seven small, closely spaced volcanic constructs. Each is composed of high SiO₂ and low FeO content rock with the

summits surfaced by the highest SiO₂ and lowest FeO content lava flows, while the lower elevation areas of MMD and parts of the central plateau appear to be composed of slightly lower SiO₂ and slightly higher FeO content materials. Some of the lowest SiO₂ and highest FeO content materials also occur along the mare/MMD contact. This may be partly due to contamination by material thrown from the mare on to MMD by the formation of nearby impact craters. This type of contamination is common along such boundaries for features of this approximate age elsewhere on the Moon, and is only important within 1 km–1.5 km of these boundaries (Logan et al., 1972; Boyce et al., 2017).

Combining crater count data with these observations suggests that volcanism at MMD started ~ 100 Ma after the formation of the Iridium basin ($\sim 3.84 \pm 0.11$ Ga; see Wagner et al., 2002) with the eruption of relatively high SiO₂ and low FeO content lavas at $\sim 3.75 \pm 0.1$ Ga. At about the same time (i.e., $\sim 3.75 \pm 0.1$ Ga), high SiO₂ lavas erupted at Mairan T dome, and likely at Mairan South dome too, while at approximately the same time ($\sim 3.73 \pm 0.1$ Ga) mare volcanism also occurred in the area. This is consistent with the model age estimated for this mare of $\sim 3.6 \pm 0.1$ Ga by Boyce (1976) based on crater degradation.

Approximately 400 My later (i.e., $\sim 3.35 \pm 0.2$ Ga), a second major episode of volcanism occurred at MMD and the surrounding mare. High SiO₂ and low FeO lavas erupted at the summits of the South and East domes on MMD during this phase. Lavas with similar compositions also may have erupted at/near the summits of the other domes and ridges on MMD at nearly the same time, but the lack of reliable crater counts in these areas make this only speculative. In addition, during this time, moderately lower SiO₂ and higher FeO content lavas (compared with those that formed the summits) erupted to form the central plateau of MMD.

At approximately the same time while this phase of silicic volcanism was in full swing, basalt (FeO $\sim 17 \pm 1$ wt. %) lava flows flooded a large area around the Mairan domes. The model age for these eruptions (i.e., $\sim 3.30 \pm 0.2$ Ga) is consistent with those measured by Boyce (1976) for maria in the area of MMD. No younger mare like those reported by Hiesinger et al. (2003) was found in the area in the vicinity of the MMD.ed was ~ 50 km to the west of the MMD. The resultant mare model age (i.e., 1.33 Ga) from these counts was extrapolated across a relatively broad area defined by uniformities in Clementine color-ratio data to include the mare surrounding Mairan domes. Hiesinger et al. (2003) assumed that the broad unit defined from Clementine color-ratio data was of both uniform composition and age. However, a close examination of their color-ratio map (and a preliminary reprocessing of the Clementine data) shows that the subtle color variations occur within the broad color unit they mapped suggesting a region of greater complexity than they initially recognized. We believe that, to a first order, this likely explains the inconsistency noted here, but clearly this subject should be investigated more thoroughly in a future study.

MMD appears to be mantled by a ~ 3 m - 4 m thick regolith that is likely produced by impact gardening of the silica-rich lava flows. Diviner rock abundance observations suggest few rocks occur in the surface of MMD, even around fresh impact craters, consistent with the observation that boulders are uncommon in high-resolution images of the surface. This lack of boulders is somewhat puzzling, but may be due to the possibility that MMD is surfaced by a thin pyroclastic mantle like observed at other lunar silicic domes (e.g., see Boyce et al., 2017), or MMD could be surfaced by materials that readily mechanically degrades into small particles by impact gardening, although neither of these alternatives is completely consistent with observations.

5. Implications to models of the origin of high Si lunar magmas

Although most data indicate a high-silica composition for the material that makes up the MMD and other similar "red spot" volcanic centers, the origin of lunar silica-rich magmas is uncertain. Models include extensive fractional crystallization of intrusions of mare basaltic magmas or KREEP magmas (e.g., Ryder, 1976; Jolliff et al., 2011). A related model is

formation of silicic magmas by silicate immiscibility after significant fractional crystallization (e.g., Hess, 1989). Both models suffer from the problem that fractional crystallization of even evolved magma, like KREEP basalt, produces only small quantities of residual, silica-rich magma. This problem led Hagerty et al. (2006) to propose an origin by heating and partial melting of KREEP crustal rock by intrusions of mare basaltic magma, perhaps involving underplating at the crust-mantle boundary. Such mechanisms have been proposed for production of silicic rocks on Earth (e.g., Bergantz, 1989). The partial melting mechanism has been verified experimentally by Gullikson et al. (2016), with certain limitations on pressure and crustal composition (with partial melting of somewhat evolved monzogabbro and gabbro-norites, derived from partial melting of KREEP basalts, and favored to produce rhyolitic composition magma).

Our study of MMD provides some independent support for the underplating mechanism, although it does not completely rule out the other models. Massive intrusions of mare basaltic magma ought to have led to at least some basaltic eruptions. If partial melting of crustal rock occurred during the large intrusive events, then silicic magmas ought to have similar ages to those of erupted mare basaltic magmas. Fig. 10 shows that the two dominant model ages for materials composing the MMD (3.75 ± 0.1 Ga and 3.35 ± 0.2 Ga) are within uncertainties of model ages of mare basalts southeast of MMD (3.73 ± 0.1 Ga) and the mare model ages north and west of MMD (3.30 ± 0.2 Ga). While not a direct test of the hypothesis that the silicic eruptive materials on the MMD were formed by partial melting of evolved crustal rock, the age correspondence is consistent with the idea. This is also an important reason for why detailed studies of other lunar silicic deposits are warranted that investigate chronological relationships between silicic units and surrounding mare units in order to provide data to test these models. However, this issue can best be resolved by analysis of returned samples from the “red spot” volcanic centers.

6. Summary and conclusion

Because of their small size and previous lack of the high-resolution imaging and remote sensing data, little was known about the geology of Mairan domes. Recent acquisition of such data from a variety of orbiting platforms and instruments such as LROC have dramatically enabled characterization and mapping of distinct geologic units on the largest of these domes, Mairan middle dome. Our findings help confirm these features to be volcanic constructs composed of high SiO₂ and low FeO lava flows, and that MMD has a much more complex geologic history than previously thought.

These data suggest that MMD was constructed in two phases, ~400 million years apart. The first episode occurred at $\sim 3.75 \pm 0.1$ Ga, shortly after the formation of the Iridium basin, when viscous, relatively low-FeO, and relatively high-silica lavas erupted at MMD. Similar volcanism also occurred at Mairan T (and likely Mairan South dome) at about the same time. Mare basaltic volcanism also occurred in the vicinity at about the same time ($\sim 3.73 \pm 0.1$ Ga). Approximately 400 million years later, a second major episode of volcanism occurred (i.e., at $\sim 3.35 \pm 0.2$ Ga), when even lower FeO, and higher silica lavas were erupted at MMD. These eruptions built the summits of the individual small volcanic massifs, and the central flat area on MMD. At about the same time ($\sim 3.30 \pm 0.2$ Ga) basaltic lavas flooded the area around MMD and Mairan T. No traces of the 1.33 Ga old mare reported by Hiesinger et al. (2003) was found in the area studied around the Mairan domes, but units with this young age may indeed exist in the area several tens of kilometers to the west of Mairan T, where the crater counts were conducted.

These findings suggest that each episode of silicic volcanism at MMD (and likely the other Mairan domes) was also accompanied by mare basaltic volcanism. The coincidental eruption of high SiO₂, and low-FeO lavas and mare basalts in this area is most consistent with the basaltic underplating mechanism proposed by Hagerty et al. (2006). In this mechanism, partial melting of KREEP basalts (driven by the heat from the

intrinsic radioactivity of KREEP and from mare basaltic intrusions) should produce significant volumes of rhyolitic magma with the right range in FeO, as well as a high thorium abundance. This is similar to volcanism at and around Mons Hansteen, where silicic lavas were erupted at about the same time large volumes of mare forming basalt lavas erupted (Boyce et al., 2017).

Acknowledgements

We would like to thank Dr. James W. Ashley and an anonymous reviewer for their thoughtful and thorough reviews. Their efforts have made this a substantially better contribution. We would like to acknowledge support by NASA's through LRO/LROC contract ASU 11–599 with Arizona State University (Mark Robinson, PI).

References

- Ashley, J.W., Robinson, M.S., Stopar, J.D., Glotch, T.D., Ray Hawke, B., Lawrence, S.J., Jolliff, B.L., Hiesinger, H., van der Bogert, C.H., Greenhagen, B.T., Giguere, T.A., Paige, D.A., 2016. The Lassell massif — a silicic lunar volcano. *Icarus* 273, 248–261.
- Bergantz, G.W., 1989. Underplating and partial melting: implications for melt generation extraction. *Science* 245 (4922), 1093–1095.
- Boyce, J.M., 1976. Ages of flow units in the lunar nearside maria based on Lunar Orbiter IV photographs. Seventh Lunar Sci. Conf. *Geochim. et Cosmochim. Acta* 3 (7), 2717–2729.
- Boyce, J.M., Giguere, T.A., Hawke, B.R., Mougini-Mark, P.J., Robinson, M.S., Lawrence, S.J., Trang, D., Clegg-Watkins, R.N., 2017. Hansteen Mons: a LROC geological perspective. *Icarus*. <https://doi.org/10.1016/j.icarus.2016.08.013>.
- Chauhan, M., Bhattacharya, S., Saran, S., Chauhan, P., Dagar, A., 2015. Compton-belkovich volcanic complex (CBVC): an ash flow caldera on the moon. *Icarus* 253, 115–129.
- Chevrel, S.D., Pinet, P.C., Head III, J.W., 1999. Gruithuisen domes region: a candidate for an extended nonmare volcanism unit on the Moon. *J. Geophys. Res.* 104, 16515–16529.
- Duffield, W., Richter, D., Priest, S., 1999. Physical Volcanology of Silicic Domes as Exemplified by the Taylor Creek Rhyolite, Catron and Sierra Counties, New Mexico. U.S. Geol. Survey Prof. Paper, with MAP I-2399, U. S. G. P. O. 1995-387-030:00099, p. 20.
- Eliason, E.M., et al., 1999. Digital processing for a global multispectral map of the Moon from Clementine UVVIS imaging instrument. *Lunar Planet. Sci. [CD-ROM] XXX* abstract 1933.
- Glotch, T., Hagerty, J., Lucey, P., Hawke, B., Giguere, T., Arnold, J., Williams, J., Jolliff, B., Paige, P., 2011. The Mairan domes: silicic volcanic constructs on the Moon. *Geophys. Res. Lett.* 38, L21204 <https://doi.org/10.1029/2011GL049548>.
- Glotch, T., Lucey, P., Banfield, J., Greenhagen, B., Thomas, I., Elphic, R., Bowles, N., Wyatt, M., Allen, C., Hanna, K., Paige, D., 2010. Identification of highly silicic features on the Moon. *Science* 329, 1510–1515.
- Greenhagen, B.T., et al., 2010. Global silicate mineralogy of the moon from the diviner lunar radiometer. *Science* 329, 1507–1509.
- Gullikson, A.L., Hagerty, J.J., Reid, M.R., Rapp, J.F., Draper, D.S., 2016. Silicic lunar volcanism: testing the crustal melting model. *Am. Mineral.* 101, 2312–2321.
- Hagerty, J., Lawrence, D., Hawke, B., Vaniman, D., Elphic, R., Feldman, W., 2006. Refined thorium abundances for lunar red spots: implications for evolved, nonmare volcanism on the Moon. *J. Geophys. Res.* 111, E06002.
- Hartmann, W., Strom, R., Weidenschilling, S., Blasius, K., Woronow, A., Dence, M., Grieve, R., Diaz, J., Chapman, C., Shoemaker, G., Jones, K., 1981. Chronology of planetary volcanism by comparative studies of planetary cratering. In: McGetchin, T., Pepin, R., Phillips, R. (Eds.), *Basaltic Volcanism on the Terrestrial Planets*. Pergamon Press, New York, p. 1286.
- Hawke, B., Lawrence, D., Blewett, D., Lucey, P., Smith, G., Spudis, P., Taylor, G., 2003. Hansteen Alpha: a volcanic construct in the lunar highlands. *J. Geophys. Res.* 108 (E7), 5069. <https://doi.org/10.1029/2002JE002013>.
- Head, J.W., Hess, P.C., McCord, T.B., 1978. Geologic characteristics of lunar highlands volcanic (Gruithuisen and Mairan region) and possible eruption conditions. In: *Proc. Ninth Lunar Planet. Sci. Conf.*, pp. 488–490.
- Head, J.W., McCord, T.B., 1978. Imbrian-age highland volcanism on the moon: the Gruithuisen and Mairan domes. *Science* 199, 1433–1436.
- Hess, P.C., 1989. Highly Evolved Liquids from the Fractionation of Mare and Nonmare Basalts. Moon in Transition. LPI Tech Report 89-03. Lunar and Planetary Institute, Houston.
- Hiesinger, H., Head III, J., Wolf, U., Jaumann, R., Neukum, G., 2003. Ages and stratigraphy of mare basalts in Oceanus Procellarum, mare Nubium, mare cognitum, and mare insularum. *J. Geophys. Res.* 108 (E7), 5065. <https://doi.org/10.1029/2002JE001985>.
- Housen, K., Holsapple, K., 2012. Craters without ejecta. *Icarus* 219, 297–306.
- Isbell, C., et al., 1999. Clementine: a multispectral digital image model archive on the Moon. *Lunar Planet. Sci. XXX [CD-ROM] abstract 1812*.
- Jolliff, B., 1998. Large scale separation of K-fac and KREEP-fac in the source region of Apollo impact-melt breccia and revised estimate of the KREEP composition. *Int. Geol. Rev.* 40, 916935 <https://doi.org/10.1080/00206819465245>.

- Jolliff, B., Wiseman, S., Lawrence, S., Tran, T., Robinson, M., Sato, H., Hawke, B., Scholten, F., Oberst, J., Hiesinger, H., van der Bogert, C., Greenhagen, B., Glotch, T., Paige, D., 2011. Non-mare silicic volcanism on the lunar farside at Compton–Belkovich. *Nature Geosci.* 4, 566–571.
- Korotev, R.I., 1998. Concentration of radioactive elements in lunar materials. *J. Geophys. Res.* 103, 1691–1701. <https://doi.org/10.1038/ngeo1212>.
- Lawrence, D., Hawke, B., Hagerty, J., Elphic, W., Feldman, T., Prettyman, T., Vaniman, D., 2005. Evidence for high-Th evolved lithology on their moon at Hansteen Alpha. *Geophys. Res. Lett.* 35, L23202 <https://doi.org/10.1029/2004GL022022>.
- Logan, L., Hunt, G., Balsano, S., Salisbury, J., 1972. Mid-infrared emission spectra of Apollo 14 and 15 soils and remote compositional mapping of the moon. In: *Proc. Lunar Science Conf.*, vol. 3, pp. 3069–3076.
- Lucey, P.G., Blewett, D.T., Jolliff, B.L., 2000a. Lunar iron and titanium abundance algorithms based on final processing Clementine ultraviolet visible images. *J. Geophys. Res.* 105 (E8), 20,297–20,305. <https://doi.org/10.1029/1999JE022022>.
- Lucey, P.G., Blewett, D., Taylor, G., Hawke, B., 2000b. Images of lunar surface maturity. *J. Geophys. Res.* 105 (E8), 20,377–20,386.
- Malin, M., 1974. Lunar red spots: possible pre-mare materials. *Earth Planet Sci. Lett.* 21, 331–341.
- Michael, G.G., Neukum, G., 2010. Planetary surface dating from crater size–frequency distribution measurements: partial resurfacing events and statistical age uncertainty. *Earth Planet Sci. Lett.* 294, 223–229. <https://doi.org/10.1016/j.epsl.2009.12.041>.
- Melosh, H.J., 1989. *Impact Cratering*. Oxford University Press, New York.
- Moore, H.J., Boyce, J.M., Schaber, G.G., Scott, D.H., 1980. Lunar remote sensing and measurements. Chapter B. In: *Apollo 1517 Orbital Investigations: U.S. Geol. Survey Prof. Paper*, 10468, 78 p.
- Neukum, G., Ivanov, B.A., Hartmann, W.K., 2001. Cratering records in the inner Solar System in relation to the lunar reference system. *Space Sci. Rev.* 96, 55–86.
- Oberbeck, V.R., Quaide, W.L., 1967. Estimated thickness of a fragmental surface layer of Oceanus Procellarum. *J. Geophys. Res.* 72, 4697–4704.
- Oberbeck, V.R., Morrison, 1974. Laboratory simulations of the herringbone patterns associated with lunar secondary craters chains. *Moon* 9, 415–455.
- Paige, D.A., et al., 2010. The lunar reconnaissance orbiter diviner lunar radiometer experiment. *Space Sci. Rev.* 150, 125–160.
- Papike, J.J., Ryder, G., Shearer, C.K., 1998. Lunar samples. *Rev. Mineral.* 36, 1–189.
- Robinson, M.S., McEwen, A.S., Eliason, E., Lee, E.M., Malaret, E., Lucey, P.G., 1933. Clementine UVVIS global mosaic: a new tool for understanding the lunar crust. *Lunar Planet. Sci.* 1999 [CD-ROM], XXX, abstract.
- Robinson, M., Brylow, S., Tschimmel, M.D., Humm, D., Lawrence, S., Thomas, P., Denevi, B., Bowman-Cisneros, E., Zerr, J., Ravine, M., Caplinger, M., Ghaemi, F., Schaffner, J., Malin, M., Mahanti, P., Bartels, A., Anderson, J., 2010. Lunar reconnaissance orbiter Camera (LROC) instrument overview. *Space Sci. Rev.* 150, 81–124.
- Ryder, G., 1976. Lunar sample 15405: remnant of a KREEP basalt-granite differentiated pluton. *Earth Planet Sci. Lett.* 29, 255–268.
- Schultz, P., Greeley, R., Gault, D., 1977. Interpreting statistics of small lunar craters. In: *Proc. Lunar Sci. Conf.*, vol. 8, pp. 3539–3564.
- Scott, D.H., Eggleton, R.E., 1973. Geologic map of the rumker quadrangle of the moon. In: *U. S. Geol. Surv. Misc. Invest. Ser. Map*, vols. I-805.
- van der Bogert, C., Hiesinger, H., McEwen, A., Dunda, C., Bray, V., Robinson, M., Plescia, J., Reiss, D., Klemm, K., the LROC Science Team, 2010. Discrepancies between crater size-frequency distributions on ejecta and impact melt pools at lunar craters. *Lunar Planet Sci. XLI* [CD-ROM], Abstract 2165.
- van der Bogert, C.H., et al., 2015. Development of Guidelines for Recommended Lunar CSFD Count Area Sizes via Analysis of Random CSFDs. *Workshop on Issues in Crater Studies and the Dating of Planetary Surfaces*, Laurel, MD, #9023.
- Wagner, R., Head, J., Wolf, U., Neukum, G., 2002. Lunar red spots: stratigraphic sequence and ages of volcanic units in the Gruithuisen region of the Moon. *J. Geophys. Res.* 107 (E11), 5104. <https://doi.org/10.1029/2002JE001844>.
- Wagner, R., Head, J., Wolf, U., Neukum, G., 2010. Lunar red spots: stratigraphic sequence and ages of domes and plains in the Hansteen and Helmet regions on the lunar nearside. *J. Geophys. Res.* 115, E06015.
- Wilson, L., Head, J.W., 2003. Lunar Gruithuisen and Mairan domes: rheology and mode of emplacement. *J. Geophys. Res.* 108 (E2), 5012. <https://doi.org/10.1029/2002JE001909>.
- Wood, C.A., Head, J.W., 1975. Geologic setting and provenance of spectrally distinct premare material of possible volcanic origin. In: *Conference on Origin of Mare Basalts*, Lunar Sci. Inst., Houston, Tex (Abstract).